DOI: 10.1021/ma100719m

Macromolecules
ARTICLE

On the Origin of Slow Changes in Ionic Conductivity of Model Block Copolymer Electrolyte Membranes in Contact with Humid Air

Xin Wang,[†,⊥] Sergey Yakovlev,[‡] Keith M. Beers,[‡,⊥] Moon J. Park,[‡,⊥,∥] Scott A. Mullin,[†,⊥] Kenneth H. Downing,*[,§] and Nitash P. Balsara*[,†,‡,⊥]

[†]*Environmental Energy Technologies Division,* [‡]*Materials Sciences Division, and* [§]*Life Sciences Division, Lawrence Berkeley National Laboratory, Berkeley, California 94720, and* [⊥]*Department of Chemical Engineering, University of California, Berkeley, California, 94720.* [∥]*Department of Chemistry, Pohang University of Science and Technology, Korea*

Received April 3, 2010; Revised Manuscript Received May 11, 2010

ABSTRACT: Proton conductivity (σ) and degree of hydration (λ) of poly(styrenesulfonate−methylbutylene) (PSS−PMB) block copolymers in contact with humid air were studied as a function of temperature under high-humidity conditions (relative humidity between 90 and 98%). The volume fraction of the hydrophilic PSS block in the dry state was 0.27 ± 0.01 in all of the samples, and the size of the hydrophilic channels was varied by varying the overall molecular weight of the samples. All of the samples have a lamellar structure in the dry state. The water uptake data were unremarkable, and a degree of hydration of 14 ± 2 H_2O molecules per sulfonic acid group was obtained, regardless of temperature, thermal history, and hydrophilic channel size. In contrast, measured values of σ were highly dependent on thermal history and sample molecular weight. Equilibrated values of σ, obtained only after heating the samples to 90 °C for 48 h, were significantly lower than those obtained after initially hydrating the polymer films during the heating runs. In addition, the low molecular weight samples were more sensitive to thermal history than the high molecular weight samples. Small-angle neutron scattering and transmission electron microscopy studies on the humidified samples revealed that the low molecular weight samples undergo a transition to hexagonally perforated lamellae upon hydration while the highest molecular weight sample did not. We speculate that the slow changes in σ are due to the formation of less connected ion transporting channels or ionic clusters that impede ion motion. Equilibrated ionic conductivities increase as the hydrophilic channel size decreases.

Introduction

Fuel cell technology continues to attract attention because it holds the promise of providing an environmentally friendly power source.[1] An important component of fuel cells is the polymer electrolyte membrane (PEM) that conducts protons between the electrodes. The most widely studied PEM is Nafion, which is a linear fluoropolymer that contains a random distribution of sulfonic acid groups.[2] The proton conductivity of Nafion is intimately related to the water content in the membrane. Experimental evidence clearly shows the presence of discrete sulfur-rich hydrophilic microphases with dimensions of a few nanometers dispersed within the Nafion membrane in the dry state.[3−6] Upon exposure to humid air, water is taken up by the hydrophilic microphases, and this ultimately leads to the creation of continuous hydrophilic channels that enable proton transport through the membrane.[3,7−9]

One might expect conductivity, σ, to be closely related to degree of hydration, λ, where λ is the molar ratio of water to sulfonic acid groups in the membrane. This, however, is not the case, particularly at high humidity and temperature. Take the example of Nafion 117. There is general consensus that the value of λ for Nafion 117 in prolonged contact with air with RH = 100% is about 14 at room temperature.[8,10−14] In contrast, the reported values of σ vary from 0.001 to 0.1 S/cm.[11−20] It is evident that conductivity of Nafion can vary by 2 orders of magnitude in spite of the fact that the water content in all of the membranes is similar. It is recognized that one of the factors that contribute to the variability of σ is slow kinetics and nonequilibrium behavior.[10,21] This is not surprising because Nafion is a semicrystalline polymer, and these systems are far from equilibrium even in the dry state. One of the difficulties with Nafion is the lack of morphological information in the hydrated state. Small-angle X-ray scattering profiles from hydrated Nafion show a reproducible and well-defined peak. However, this feature alone is not enough to uniquely specify the morphology. Proposed morphologies for the hydrated channels include spherical nodules connected by cylindrical connectors,[22,23] bundles of cylindrical channels,[24] individual cylindrical channels,[25] lamellar channels,[26] and disordered networks.[27] In some studies, conductivity data are presented without reference to a model of the ion-conducting channels.[28−31]

This paper is part of a series on the properties of model PEMs obtained from polystyrenesulfonate-*block*-polymethylbutylene (PSS−PMB) copolymers.[32−36] Our previous studies were restricted to symmetric samples wherein the volume fraction of PSS was in the vicinity of 0.5. The present study represents the start of our work on asymmetric PSS−PMB copolymers with a PSS volume fraction of about 0.27. We present measurements of σ and λ as a function of time and temperature from a series of samples with varying total molecular weights. We demonstrate that σ of these samples is highly dependent on sample history while λ is not. In this respect, asymmetric PSS−PMB copolymers are similar to Nafion. In contrast, both σ and λ of symmetric PSS−PMB copolymers were not sensitive functions of sample history provided waiting times of 24−48 h were used to record the data.[30] In an attempt to understand the origin of the history dependence of σ, the morphology of hydrated asymmetric PSS−PMB copolymers was determined by a combination of *in situ* small-angle neutron scattering (SANS) under humidity control and cryogenic transmission electron microscopy (TEM) of hydrated samples.

*Corresponding author. E-mail: nbalsara@berkeley.edu.

 Published on Web 05/28/2010

Table 1. Characteristics of Polymers Used in This Study

	PS-*b*-PMB precursor information						
sample code	MW (kg/mol)	PDI	ϕ_{PS}	SL (%)	ϕ_{PSS}	IEC (mmol/g)	dry state morphology (25 °C)
A2	1.6−4.0	1.03	0.25	42	0.27	1.04	lamellae
A3	3.2−8.1	1.02	0.25	41	0.27	1.03	lamellae
A6	5.9−13.4	1.03	0.27	40	0.28	1.07	lamellae

Experimental Section

Sample Synthesis and Characterization. Poly(styrene-*b*-methylbutylene) (PS−PMB) copolymers with PS volume fraction of about 0.25 were synthesized by sequential anionic polymerization of styrene and isoprene, followed by selective hydrogenation of the polydiene,[37,38] followed by sulfonation of the PS block to yield poly(styrenesulfonate-*b*-methylbutylene) (PSS−PMB) block copolymers.[39] While the extent of sulfonation was controlled, the locations of the sulfonic acid groups were not. The sulfonic acid groups are thus expected to be more or less randomly distributed within the PSS block.

The sulfonation level (SL), defined by eq 1, was determined by ^{1}H NMR in d_8-THF solution. Ion exchange capacity (IEC) in eq 2 quantified as the moles of sulfonic acid group per gram of polymer (mmol/g) was calculated from SL and the molecular weight of the copolymer. Details concerning synthesis and characterization of our polymers are given in ref 33. The characteristics of the samples used in this study are given in Table 1.

$$\mathrm{SL} = \frac{\text{mol of SSA}}{\text{mol of S} + \text{mol of SSA}} \tag{1}$$

$$\mathrm{IEC} = \frac{1000 \times \text{mol of SSA}}{\text{mol of SSA} \times \mathrm{MW_{SSA}} + \text{mol of S} \times \mathrm{MW_S} + \text{mol of MB} \times \mathrm{MW_{MB}}} \tag{2}$$

where SSA is styrenesulfonic acid, S is styrene, MB is methylbutylene, and MW is molecular weight of the SSA, S, and MB monomers in g/mol.

Small-Angle X-ray Scattering. Samples for synchrotron small-angle X-ray scattering (SAXS) measurement were prepared by solvent casting from 15 wt % THF solution in a 1 mm thick spacer. Samples were dried in a fume hood for 3 days and then vacuum-dried until the weight did not change. SAXS was performed at beamline 7.3.3 at the Advanced Light Source (ALS) at Lawrence Berkeley National Laboratory. Samples were equilibrated for 15 min at the temperature of interest before measurements were made. The original two-dimensional scattering images were azimuthally averaged to generate one-dimensional scattering intensity profiles, $I(q)$, where the magnitude of the scattering wave vector $q = 4\pi \sin(\theta/2)/\lambda$, where θ is scattering angle and λ is the wavelength of the incident beam.

Conductivity. Free-standing sample films with dimension 2 cm × 1 cm × 200 μm were prepared for conductivity measurements by solvent-casting from 15 wt % THF solutions. Films were carefully dried without introducing bubbles. The thickness of sample films was measured using a micrometer. In-plane proton conductivity of hydrated membranes was measured by ac impedance spectroscopy using platinum electrodes in the standard four-probe configuration using a BekkTech sample clamp. Data were collected over a frequency range of 0.2 Hz−100 kHz in a humidity- and temperature-controlled oven (SH-241, Espec. Corp). Conductivity, σ, is given by

$$\frac{1}{\sigma} = \frac{rS}{w} \tag{3}$$

where S is the cross-sectional area of sample film, r is the touch down of the Nyquist semicircle on the real axis, and w is the distance between the inner platinum electrodes.

Water Uptake. 200 μm thick polymer films were prepared by solvent-casting from a 15 wt % THF solution (20 mg of polymer). The films were dried in a fume hood at room temperature for 3 days and then dried in a vacuum oven at room temperature until the weight of the film was constant. The dry sample weights were measured immediately after they were removed from the vacuum oven. The dry film was then hooked on the end of a Ruska fused-quartz spring, which was held in a glass tube with an open end to avoid rotation and breakage due to the air flow in a SH-241 humidity-controlled oven. The spring extension was measured through an open window in the oven by a cathetometer equipped with an optical zoom telescope located outside the oven. Care was taken to minimize the time when the window was opened (typically 15 s). The spring was calibrated with standard masses at experimental temperatures and relative humidity in the chamber before use (spring constant was about 0.5 mg force/mm). Water uptake, W, is defined as the ratio of the weights of the sample after water uptake to that of the dry film weight, as shown in eq 4.

$$W = \frac{\text{hydrated film weight} - \text{dry film weight}}{\text{dry film weight}} \times 100\% \tag{4}$$

The degree of hydration, λ, defined as the moles of water per mole of sulfonic acid groups in the membrane, is calculated using eq 5

$$\lambda = \frac{[\mathrm{H_2O}]}{[\mathrm{SO_3^-}]} = \frac{\text{water uptake (\%)} \times 10}{\mathrm{MW_{H_2O}} \times \text{IEC (mmol/g)}} \tag{5}$$

where $\mathrm{MW_{H_2O}} = 18.02$ g/mol.

***In-Situ* Small-Angle Neutron Scattering.** Samples for SANS were prepared by solvent-casting polymer from 10% THF solutions on 1 mm thick quartz windows. Sample thickness ranged from 90 to 120 μm, and a circular area with diameter of 1.6 cm was exposed to the neutron beam. Samples were studied on the NG7 and NG3 beamlines at the National Institute of Standard and Technology (NIST) in Gaithersburg, MD, using a humidity- and temperature-controlled sample stage. Pure D_2O placed in the two reservoirs of the chamber was used to control the humidity. The wavelength of the incident neutron beam was 0.6 nm, and sample-to-detector distances of 5.0 and 13.0 m were used. The raw data were converted to absolute coherent scattering intensity, I, as a function of scattering wave vector q ($q = 4\pi \sin(\theta/2)/\lambda$, where θ is the scattering angle and λ is the wavelength of the incident neutrons) after corrections for detector sensitivity, background, empty cell, and incoherent scattering were applied, using standard procedures and software established by NIST.

Cryogenic Transmission Electron Microscopy. Samples for cryogenic TEM were filled in standard open copper capillary tubes (Leica) and then placed into the SH-241 humidity chamber at RH = 98%. The samples were then heated in a stepwise manner to 90 °C using a protocol that was identical to that used for the water uptake and conductivity measurements. The tubes were then removed from the oven, plunged rapidly into the liquid ethane, and stored under liquid nitrogen. Sections of the polymer were cut on a cryomicrotome (Lieca EM FC6) at −120 °C. First, the copper tube was trimmed away with a diamond knife then sections of polymer were cut. The thickness of the sections was set to 75 nm. Sections were sandwiched between two sides of

oyster TEM grids with a lacy carbon support film. Sections were stored under liquid nitrogen and transferred into the microscope using a cryo-transfer stage (Gatan). Electron micrographs were obtained on a Phillips CM 200 FEG transmission electron microscope using 200 keV acceleration voltage at −170 °C.

Results and Discussion

I. Morphology in Dry State. SAXS data obtained from the dry PSS−PMB block copolymers as a function of increasing temperature are shown in Figure 1. Primary scattering peaks at $q = q^*$ and a second-order peak at $q = 2q^*$ are seen in all of the samples over the entire temperature window. These data indicate the presence of a lamellar phase in samples A2, A3, and A6 between 25 and 112 °C. Additional higher order peaks at $q = 3q^*$ and $q = 4q^*$ are seen at 112 °C. We attribute this to annealing of the samples which generally leads to an increase in the long-range order. Lamellar microphases are typically not found in uncharged block copolymers with $f = 0.27$. However, in our previous studies on symmetric PSS−PMB copolymer, we also found microphases that are very different from those found in symmetric uncharged block copolymers.[33,40]

II. Time Evolution of Conductivity and Water Uptake. The lamellar samples A2, A3, and A6 were placed in the humidity-controlled oven at RH = 98% and subjected to the thermal history described in Figure 2. Water uptake and conductivity measurements were made in separate experiments. We first describe data obtained from A2 wherein the sample temperature was increased in steps from room temperature to 90 °C. The sample was held at each temperature for 24 h except for step 5, the step from 80 to 90 °C, where the sample was held for 48 h. It takes about 20 min for the oven to equilibrate after the temperature set point is changed. Typical time-dependent data thus obtained are shown in Figure 3. The data obtained during the step 2, after the sample temperature was increased from 25 to 40 °C, approach steady values ($W = 28\%$ and $\sigma = 0.066$ S/cm) after about 8 h, as shown in Figure 3a. Data obtained during step 4, when the temperature is changed from 60 to 80 °C, shown in Figure 3b, are qualitatively different from those shown in Figure 3a. W increases with time, saturating at 29% after about 8 h, while σ does not reach a steady value even after waiting for 24 h. In Figure 3c, we show data obtained during step 5. Here we see that W reaches a steady-state value of 28% relatively quickly while σ decreases slowly from its initial value of 0.08 S/cm, ultimately reaching a steady value of 0.038 S/cm after 44 h. Returning the sample from 90 to 25 °C in step 6 results in a decrease in σ to 0.013 S/cm, which is significantly lower than 0.054 S/cm, the value obtained at the end of step 1 at 25 °C. It appears that the heating history in the presence of humidified air has fundamentally altered the nature of the hydrophilic channels in A2. Such effects are not seen when dry A2 is heated over a similar temperature range (Figure 1).

The trends of W and σ with time in the cooling portion of the thermal history shown in Figure 2 were simpler than those seen during the heating cycle. Reheating the sample from 25 to 90 °C in step 7 resulted in steady-state W and σ values comparable to those obtained at the end of step 5. There was little change in the steady-state values of W with temperature as the temperature was decreased, while σ decreased with decreasing temperature. Steady state was achieved in all cases in 8 h or less. This is illustrated in Figure 3d where we show data obtained during step 8 after the sample temperature was changed from 90 to 80 °C.

The values of σ obtained at specific annealing times ($t = 5$, 12, and 24 h) for A2 are shown in Figure 4a. During the heating cycle, σ at a given temperature depends on annealing time,

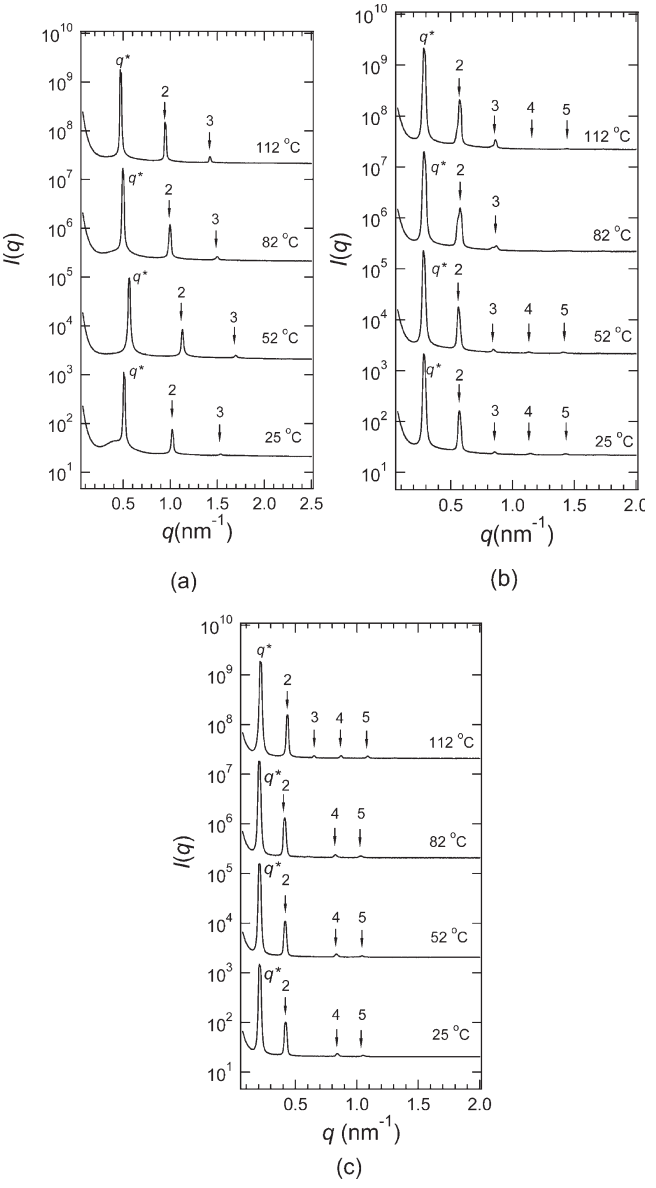

Figure 1. SAXS intensity, I, versus scattering vector, q, of samples A2 (a), A3 (b), and A6 (c) at selected temperatures in the dry state. The locations of the primary peak (q^*) and higher order peaks corresponding to a lamellar phase are indicated by arrows in the figure. Each figure has four profiles, and the intensity is multiplied by factors of 10^2 (52 °C), 10^4 (82 °C), and 10^6 (112 °C).

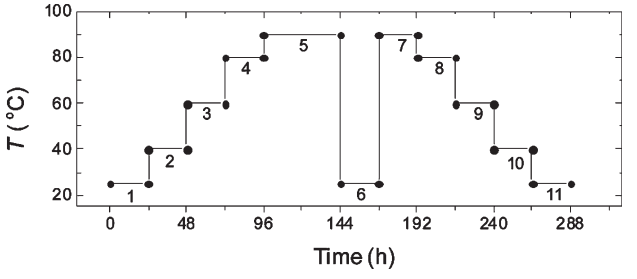

Figure 2. Thermal history used for conductivity and water uptake experiments at RH = 98%.

particularly at 80 and 90 °C. In contrast, σ at a given temperature is independent of annealing time during the cooling cycle as shown in Figure 4a. Obtaining data that are independent of annealing time is a necessary (not sufficient) condition for

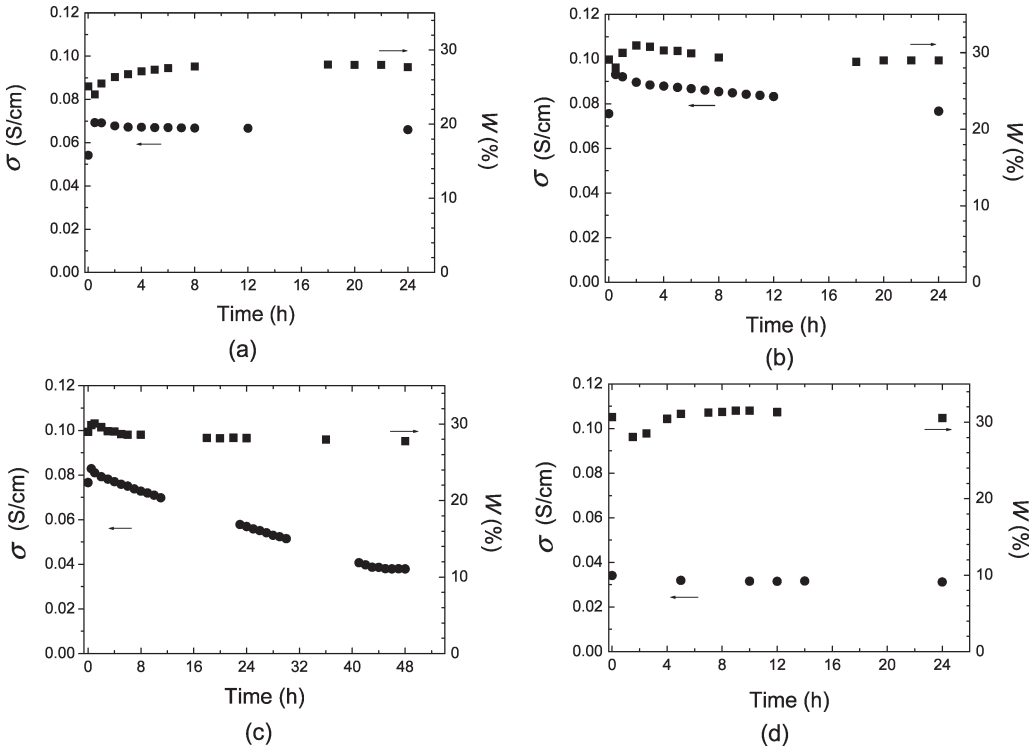

Figure 3. Time evolution of conductivity (●) and water uptake (■) of sample A2 at 40 °C, step 2 (a); 80 °C, step 4 (b); 90 °C, step 5 (c); and 80 °C, step 8 (d). See Figure 2 for definition of each step. All the measurements were conducted at RH = 98%. The conductivity and water uptake measured at the end of the previous step prior to changing the temperature set point on the humidity oven are shown at $t = 0$ h.

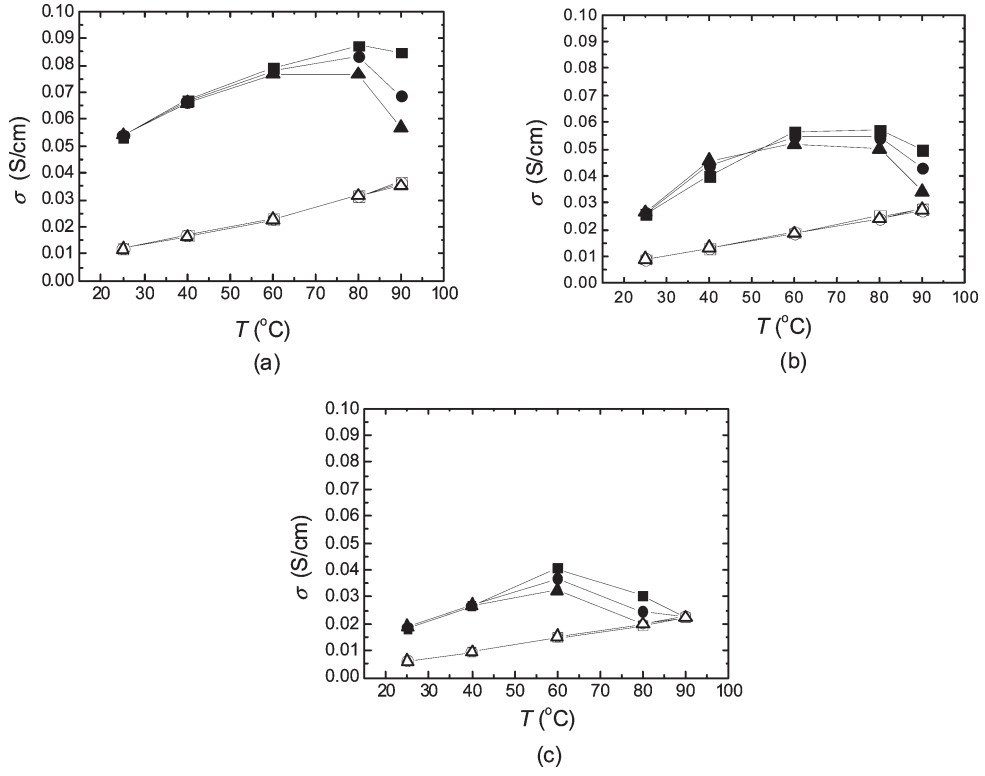

Figure 4. Temperature dependence of conductivity, σ, of samples A2 (a), A3 (b), and A6 (c) at 5 h (square), 12 h (circle), and 24 h (triangle) during heating (filled symbol) and cooling (open symbol) runs.

establishing that a sample is at equilibrium. We propose that the heating A2 in humid air at 90 °C enables equilibration. In order to further confirm that only heating to 90 °C is necessary for equilibration, we heated A2 directly to 90 °C from 25 °C, held it at that temperature for 94 h, and then cooled it to 25 °C. The value of σ thus obtained was indistinguishable from the cooling run data reported in Figure 4a.

The thermal history in Figure 2 was repeated with samples A3 and A6, and the temperature dependence of σ obtained at annealing times (t = 5, 12, and 24 h) is shown in parts b

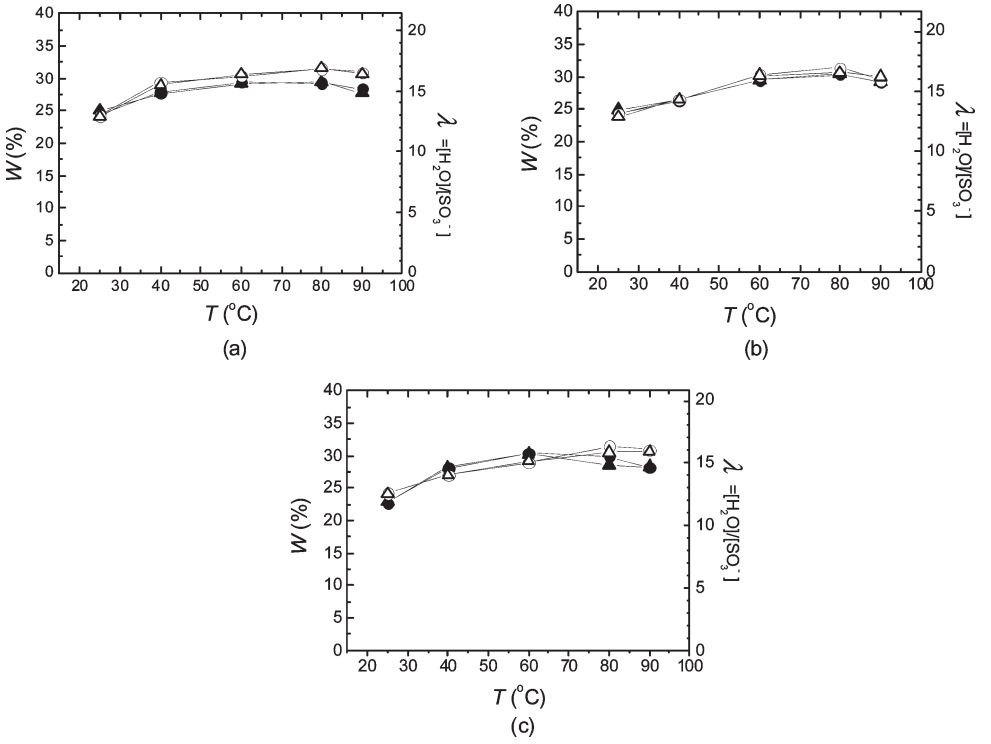

Figure 5. Temperature dependence of water uptake, W, and corresponding degree of hydration, λ, of samples A2 (a), A3 (b), and A6 (c) at 12 h (circle) and 24 h (triangle) during heating (filled symbol) and cooling (open symbol) runs.

and c of Figure 4, respectively. The data obtained from these samples are qualitatively similar to those obtained from A2. The conductivity values obtained during the heating cycles depend on annealing time while those obtained during the cooling cycle were independent of annealing time. We again propose the data obtained during the cooling run corresponds to equilibrium behavior. In the case of A3, the heating annealing from 60 to 80 °C with 24 h step time results in a steady state $\sigma = 0.034$ S/cm, which is only slightly higher than the equilibrium value of 0.028 S/cm. In the case of A6, the heating and cooling cycle data obtained at 90 °C are within experimental error, indicating that equilibrium is also obtained in the heating cycle at high temperatures in this case.

In Figure 5 we show the temperature dependence of W after 12 and 24 h during heating and cooling cycles for samples A2, A3, and A6. In sharp contrast to the conductivity data (Figure 4), the water uptake data in Figure 5 are nearly independent of thermal history. This indicates that equilibration of the overall water concentration in the block copolymers occurs relatively rapidly. It is clear that the complex time and history dependence of the conductivity is not related to water uptake.

In parts a and b of Figure 6, we show the temperature dependence of the equilibrated values of the degree of hydration and conductivity, λ_e and σ_e, respectively, for A2, A3, and A6 obtained from the cooling runs. The value of λ_e obtained in our asymmetric PSS−PMB samples is 14 ± 2, regardless of sample molecular weight or temperature (Figure 6a). In contrast, $\sigma_e(T)$ depends on sample molecular weight and follows an Arrhenius relationship (Figure 6b); $\sigma_e = A \exp(-E_a/RT)$. Arrhenius fits through the data with A and E_a as adjustable parameters led to the following estimates for A in units of S/cm: 4.9± 0.3 (A2), 3.2 ± 0.8 (A3), and 5.2 ± 2.8 (A6), and E_a in units of kJ/mol: 14.9 ± 0.2 (A2), 14.3 ± 0.7 (A3), and 16.4 ± 1.3 (A6). The fits indicates that the activation energy is nearly independent molecular weight. Using a fixed average value of E_a = 15.2 kJ/mol, we obtain the following revised estimates of A in units of S/cm: 5.44 ± 0.06 (A2), 4.33 ± 0.15 (A3), and 3.35 ± 0.28 (A6). The lines in Figure 6b represent least-squares fits with a fixed E_a.

It is obvious that the slow changes in conductivity of the samples observed during the heating run are related to the fact that our samples are out of equilibrium. Polymer systems often fall out of equilibrium due to slow molecular motion. Since molecular motion slows down with increasing molecular weight, one expects nonequilibrium behavior in high molecular weight samples. The data in Figure 4 show the opposite trend: the difference between the out-of-equilibrium heating runs and the equilibrated cooling runs is much greater in low molecular weight A2 than in the high molecular weight A6. It is clear that the origin of the slow conductivity changes observed in A2 cannot be attributed to slow molecular motion. We suspected that the reason for the slow changes in conductivity may be related to sample morphology changes that occur under humid conditions. The SANS and TEM experiments described below were designed to study the morphology of A2, A3, and A6 under controlled humidity.

III. Morphology Determination under Controlled Humidity. Sample A2 was placed in the SANS humidity chamber at 25 °C and RH = 90% (the highest RH value attainable in the instrument), and SANS profiles were recorded as a function of time. Results from this experiment are shown in Figure 7. At early time (5 min) we see a primary scattering peak at $q = q^* = 0.5$ nm^{-1} and a second-order peak at $q = 2q^*$ that are qualitatively similar to the A2 SAXS data from the dry sample shown in Figure 1a. With increasing time, however, the primary peak shifts to 0.4 nm^{-1} in a period of 24 h. Because of limited access to the neutron beam, the sample was not kept in the beam for 24 h but quickly transferred to a separate controlled humidity chamber: a closed jar containing a saturated KNO_3 solution with RH = 90.5%. (It should be evident that the thermal histories described in Figure 2 cannot be implemented on a SANS instrument due to limited beam time.) From the presence of scattering peaks at $q = 3^{1/2}q^*$ and $q = 2q^*$, it is clear that the new microphase formed after

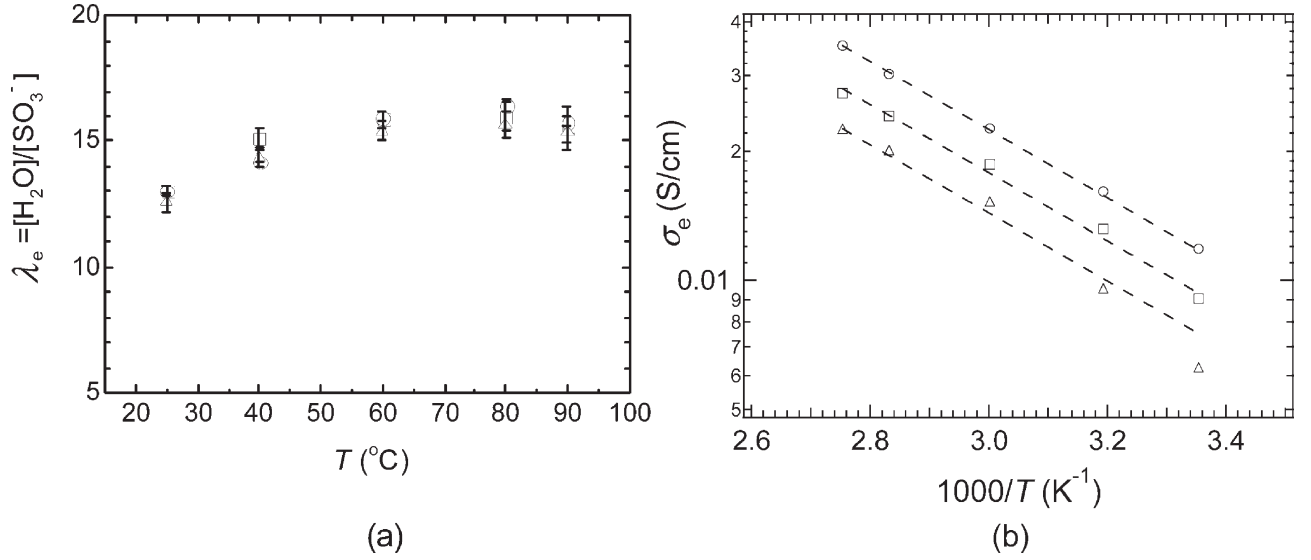

Figure 6. (a) Temperature dependence of equilibrated degree of hydration λ_e. (b) Plot of equilibrated conductivity, σ_e, vs $1000/T$. The lines through the data points are fits assuming a fixed activation energy of 15.2 kJ/mol. A2 (○), A3 (□), and A6 (Δ).

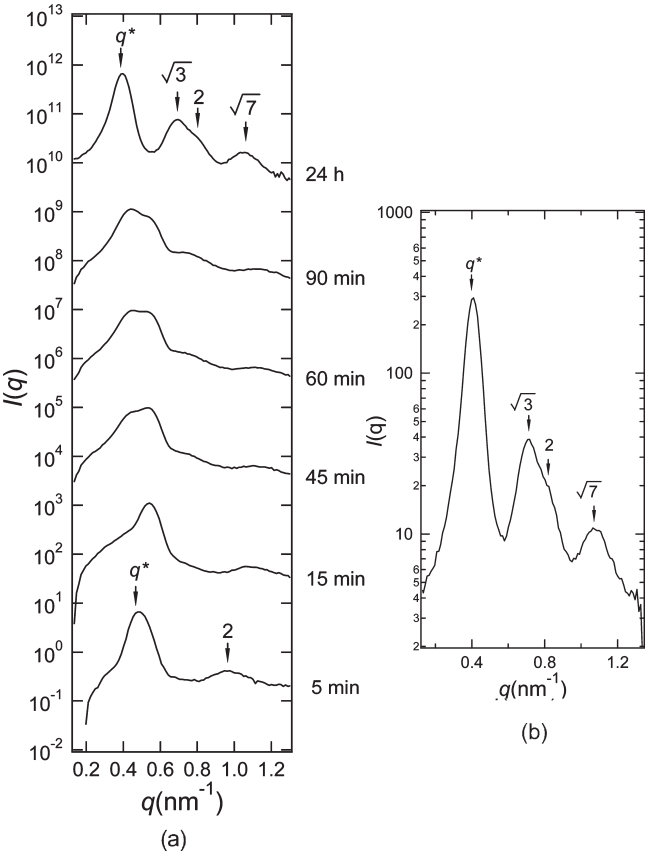

Figure 7. SANS intensity, I, vs scattering vector, q, of sample A2. (a) Data obtained after a dry sample was placed in the humidity chamber at 25 °C and RH = 90%. The profiles are offset vertically for clarity. (b) SANS data obtained at 60 °C and RH = 90%, after preannealing and rehydrating the sample. An HPL phase is seen at the end of the experiment in (a) and in (b).

exposure to humid air is not lamellar. Both hexagonally perforated lamellae (HPL) and hexagonally packed cylinders are consistent with the scattering data. For convenience, and for reasons that will become obvious soon, we will refer to the new microphase formed under humid conditions as HPL.

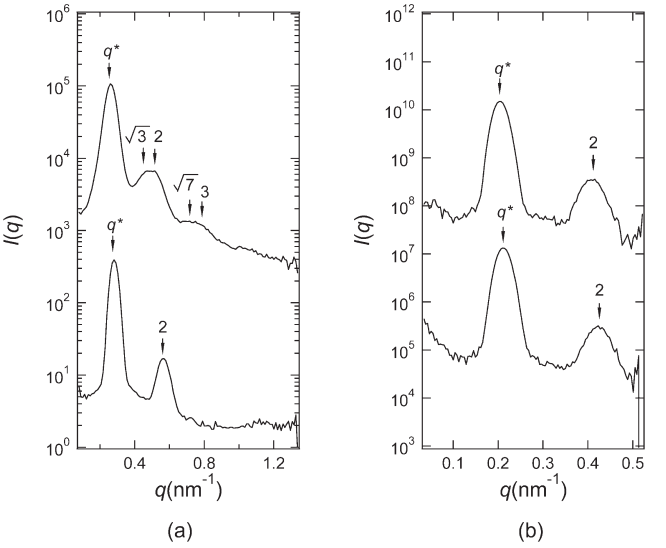

Figure 8. SANS intensity, I, vs scattering vector, q, at RH = 90% and 25 and 60 °C of samples (a) A3 and (b) A6.

Samples that were preannealed at 90 °C and RH = 98% in the controlled humidity oven, cooled to room temperature, transported to NIST, and rehydrated at the SANS instrument showed SANS profiles that are very similar to the 24 h data shown in Figure 7a. An example of this is shown in Figure 7b, where we show the SANS profile obtained from a preannealed and rehydrated sample after equilibration in the SANS humidity oven at 60 °C and RH = 90%. Once the HPL phase is formed, it appears that changing the sample temperature does not affect morphology. SANS data obtained from sample A2 at 70 °C and RH = 90% (after obtaining the data in Figure 7b) are shown in the Supporting Information.

SANS data obtained from A3 after exposure to humid air at RH = 90% at 25 and 60 °C are shown in Figure 8a. The data are qualitatively similar to those obtained from sample A2. We see a primary SANS peak at $q = q^* = 0.28$ nm^{-1} and a second-order peak at $q = 2q^*$ at 25 °C which are qualitatively similar to the A3 SAXS data from the dry sample shown in Figure 1b. Upon heating the sample to 60 °C, we see a shift in q^* to a significantly lower value and the emergence

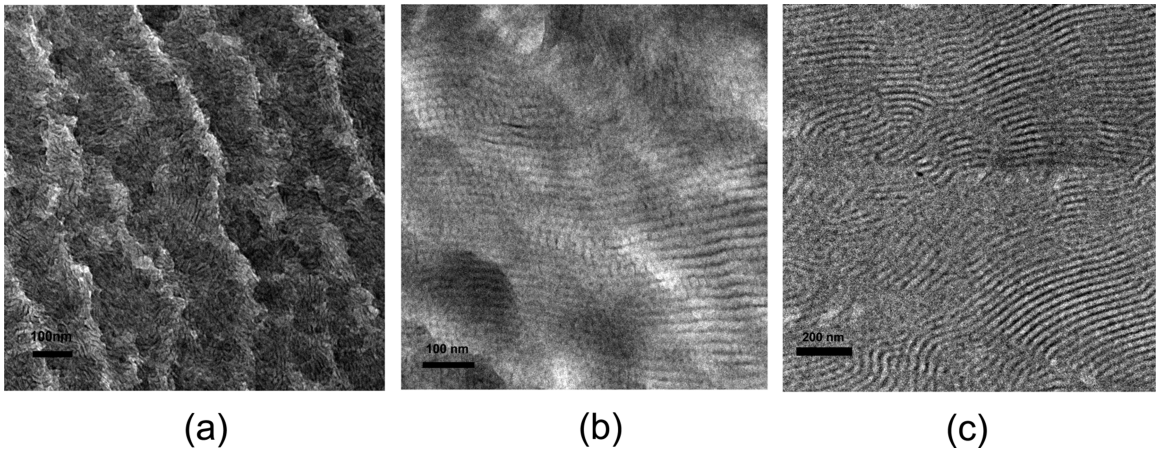

Figure 9. Cryogenic TEM images of samples (a) A2, (b) A3, and (c) A6 after step 5 at 90 °C and RH = 98%. Samples were directly quenched into liquid ethane after equilibration with humid air, sectioned, and imaged without staining.

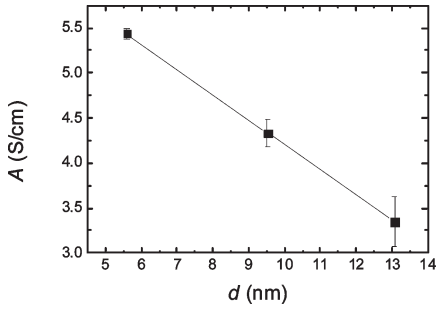

Figure 10. Plot of A, the prefactor from Arrhenius fits of temperature dependence of conductivity, vs the hydrophilic domain size d for samples A2, A3, and A6.

of higher order peaks at $q = 3^{1/2}q^*$ and $q = 2q^*$, indicating the presence of an HPL phase.

SANS data obtained from A6 after exposure to humid air at RH = 90% at 25 °C for about 50 h followed by heating to 60 °C are shown in Figure 8b. In contrast to A2 and A3, we see exposing A6 to humid air does not result in morphological changes. We see a primary SANS peak at $q = q^* = 0.21$ nm^{-1} and a second-order peak at $q = 2q^*$ which are qualitatively similar to the A6 SAXS data from the dry sample shown in Figure 1c. Sample A6 forms a lamellar microphase regardless of temperature and humidity.

In Figure 9 we show TEM results obtained from hydrated A2, A3, and A6 samples. Note that the contrast between the hydrophilic and hydrophobic phases arises only from the higher electron density of the hydrophilic phase and not due to staining as is typical of TEM experiments on polymers. In spite of this, the general features of the morphologies are evident. Sample A6 clearly shows a lamellar phase with a spacing of 30 nm, which is consistent with the SANS data. Sample A3 clearly shows an HPL phase with a spacing of 24 nm, which is consistent with the SANS data. Note that many portions of the micrographs of A3 show simple lamellae; the HPL phase is only evident when the slice happens to go through the perforations, as is the case in some portions of Figure 9b. We had considerable difficulty sectioning sample A2. This is presumably due to the low molecular weight of the sample and the presence of a soft PMB phase that forms the majority phase (water softens the hydrophilic phase). The best sections we were able to obtain from sample A2 are shown in Figure 9a. The section shows the existence of a lamellar phase, but we were unable to find regions that clearly showed the presence of perforations. In this case, we rely on the SANS profiles to infer the presence of the HPL phase and use the TEM micrographs to rule out the presence of cylinders packed on a hexagonal lattice.

The volume fraction of PSS, ϕ_{PSS}, was calculated using pure component densities of polystyrene, $\rho_{PS} = 1.05$ g/cm^3, fully sulfonated polystyrene, $\rho_{PSS} = 1.44$ g/cm^3, and poly(methylbutylene), $\rho_{PMB} = 0.86$ g/cm^3, ignoring volume changes of mixing.[41,42] Assuming that all of the water molecules are sequestered in the hydrophilic phase, we estimate that the volume fraction of the hydrophilic phase in all of our samples is about 0.41. In other words, the hydrophilic phase is the minor component in the hydrated PSS−PMB samples. It is clear from Figure 9b that the perforations are dark, indicating that the hydrophilic phase perforates the PMB lamellae. In contrast, in the well-studied case of melts of uncharged diblock copolymers, the component with volume fraction greater than 0.5 forms perforations.[43,44]

In Figure 10, we plot that value of A, the prefactor from Arrhenius fits of the temperature dependence of conductivity, obtained from the fixed E_a analysis as a function of size of the hydrophilic domains, d. For consistency, we assume that the domain size d is approximately given by $0.41(2\pi/q^*)$ (nm), ignoring the fact that the hydrophilic domains of the HPL phase have two characteristic lengths. The reported value of A in Figure 10 corresponds to a fixed value of λ of about 14. It is evident that A increases as channel size decreases. This may reflect an increase in the concentration of dissociated H^+ ions, a change in the attempt frequency for ion motion, or differences in the arrangement of water molecules inside the channels.[45] It is important to note that incomplete dissociation of H^+ ions in channels composed of polyelectrolytes can, in principle, occur at degrees of hydration as high as 14 due to effects such counterion condensation due to the proximity of the ionic species.[46,47]

Concluding Remarks

The combination of SANS, TEM, conductivity, and water uptake measurements on asymmetric PSS−PMB copolymers allow us to make the following conclusions:

1. Obtaining steady, history-independent values of σ over a limited range of thermal histories does not imply equilibrium. This is clear from Figure 4 where all data obtained during the heating runs with annealing times of 5, 12, and 24 h gave the same value of σ from 25 to 60 °C. We determined, however, that the samples were out of equilibrium during the heating runs.

2. Samples A2 and A3 wherein σ was highly history dependent also exhibited large changes in morphology upon hydration.

Sample A6 wherein σ was weakly history dependent showed no change in morphology upon hydration. The combination of SANS and TEM under humidity control was essential for establishing this.

3. The time and temperature windows over which changes in morphology are observed are similar to those over which changes in water uptake are observed. For example, the morphological changes in sample A2 at 25 °C occur on a time scale of about 24 h at room temperature (Figure 7a). This implies that the morphology change from lamellae to HPL takes place during the first step of the heating run (Figure 4). We have, however, determined the conductivity of sample A2 is far from its steady-state value at 25 °C after step 1. It is evident that slow changes within the equilibrated HPL morphology that we have not yet characterized are responsible for the changes in conductivity.

4. It is clear that some feature of the hydrophilic channels of A2 and A3 change qualitatively when the sample is annealed in a humid environment at 90 °C. Unfortunately, none of our measurements are sensitive to this feature. We can thus only speculate about the origin of the slow changes in conductivity. In the early stages of hydration (steps 1−3 in Figure 2), the H^+ ions are highly mobile. Upon further exposure to heat and humidity, however, the H^+ ions appear to be trapped in regions of low mobility. We propose that this is either due to changes in the connectivity of the ion-conducting channels or due to clustering of the H^+ ions in the hydrated state. We are not aware of any previous studies that have examined the connectivity of ion-conducting channels in PEMs directly. On the other hand, extensive studies of ionomers in the dry state indicate that the H^+ and SO_3^- ions form ion pairs that are clustered in domains that are about 4 nm in size.[22,48−52] It is conceivable that similar clusters also form at equilibrium in the hydrated state. The SO_3^- groups in our polymer are, however, located at random locations along the PSS backbone. The formation of equilibrated clusters may thus require large scale motion of polymer chains so that chains with complementary sequences are in the vicinity of each other. Difficulties of forming equilibrium morphologies in random copolymers has been noted in prior studies.[53] We argue that the formation of equilibrated clusters occurs more rapidly when hydration is not accompanied by an order−order phase transition, as is the case with sample A6.

It is clear that further work is necessary to establish the underpinnings of the slow evolution of conductivity in hydrated polymer membranes.

Acknowledgment. This work was supported by the Director, Office of Science, Office of Basic Energy Sciences, Materials Sciences and Engineering Division and the Fuel Cell Technologies Program, Energy Efficiency and Renewable Energy Division of the U.S. Department of Energy under Contract DE-AC02-05CH11231. The SAXS was performed at the Advanced Light Source, Lawrence Berkeley National Laboratory, which is a national user facility supported by the Department of Energy, Office of Basic Energy Sciences. We thank Dr. John Kerr for valuable input and guidance on the project. The SANS facilities at NIST are supported in part by the National Science Foundation under Agreement DMR-0454672.39.

Supporting Information Available: SANS profiles for A2 at 70 °C, RH = 90%; A3 and A6 at 60 °C, RH = 90% after preannealing and rehydrating samples. This material is available free of charge via the Internet at http://pubs.acs.org.

References and Notes

(1) Fuel Cell Technology and Applications. Vielstich, W., Gasteiger, H. A., Lamm, A., Eds.; *Handbook of Fuel Cell-Fundamentals, Technology and Applications*; John Wiley & Sons: New York, 2003; Vol. *3*, p 420.
(2) Curtin, D. E.; Lousenberg, R. D.; Henry, T. J.; Tangeman, P. C.; Tisack, M. E. *J. Power Sources* **2004**, *131*, 41.
(3) Mauritz, K. A.; Moore, R. B. *Chem. Rev.* **2004**, *104*, 4535.
(4) Xue, T.; Trent, J. S.; Osseo-Asare, K. *J. Membr. Sci.* **1989**, *45*, 261.
(5) Porat, Z.; Fryer, J. R.; Huxham, M.; Rubinstein, I. *J. Phys. Chem.* **1995**, *99*, 4667.
(6) Li, J.; Zhang, S.; Zhang, P.; Liu, D.; Guo, Z.-X.; Ye, C.; Zhu, D. *Chem. Mater.* **2003**, *15*, 4739.
(7) Matsuyama, M.; Kokufuta, E.; Kusumi., T.; Harada, K. *Macromolecules* **1980**, *13*, 198.
(8) Weber, A. Z.; Newman, J. *J. Electrochem. Soc.* **2003**, *150*, A1008.
(9) Viswanathan, R.; Heaney, M. *Phys. Rev. Lett.* **1995**, *75*, 4433.
(10) Onishi, L. M.; Prausnitz, J. M.; Newman, J. *J. Phys. Chem. B* **2007**, *111*, 10166.
(11) Zawodzinski, T. A.; Springer, T. E.; Uribe, F.; Gottesfeld, S. *Solid State Ionics* **1993**, *60*, 199.
(12) Simtha, B.; Sridhar, S.; Khan, A. A. *J. Membr. Sci.* **2005**, *259*, 10.
(13) Zawodzinski, T. A.; Derouin, C.; Radzinski, S.; Sherman, R. J.; Smith, V. R.; Springer, T. E.; Gottesfeld, S. *J. Electrochem. Soc.* **1993**, *140*, 1041.
(14) Mooris, D. R.; Sun, X. *J. Appl. Polym. Sci.* **1993**, *50*, 1445.
(15) Fontanella, J. J.; McLin, M. G.; Wintersgill, M. C. *Solid State Ionics* **1993**, *66*, 1.
(16) Sone, Y.; Ekdunge, P.; Simonsson, D. *J. Electrochem. Soc.* **1996**, *143*, 1254.
(17) Alberti, G.; Casciola, M.; Massinelli., L.; Bauer, B. *J. Membr. Sci.* **2001**, *185*, 73.
(18) Xie, Z.; Song, C.; Andreaus, B.; Navessin, T.; Shi, Z.; Zhang, J.; Holdcroft, S. *J. Electrochem. Soc.* **2006**, *153*, E173.
(19) Halim, J.; Buchi, F. N.; Hass, O.; Stamm, M.; Scherer, G. G. *Electrochim. Acta* **1994**, *39*, 1303.
(20) Anantaraman, A. V.; Gardner, C. L. *J. Electroanal. Chem.* **1996**, *414*, 115.
(21) Hickner, M. A.; Ghassemi, H.; Kim, H. Y.; Einsla, B. R.; McGrath, J. E. *Chem. Rev.* **2004**, *104*, 4587.
(22) Gierke, T. D.; Munn, G. E.; Wilson, F. C. *J. Polym. Sci., Polym. Phys. Ed.* **1981**, *19*, 1687.
(23) Hsu, W. Y.; Gierke, T. D. *J. Membr. Sci.* **1983**, *13*, 307.
(24) Gebel, G.; Diat, O. *Fuel Cells* **2005**, *2*, 261–276.
(25) Schmidt-Rohr, K.; Chen, Q. *Nat. Mater.* **2008**, *7*, 75.
(26) Haubold, H.-G.; Vad, Th.; Jungbluth, H.; Hiller, P. *Electrochim. Acta* **2001**, *46*, 1559.
(27) Kim, M.-H.; Glinka, C. J.; Grot, S. A.; Grot, W. G. *Macromolecules* **2006**, *39*, 4775.
(28) Lafitte, B.; Karlsson, L. E.; Jannasch, P. *Macromol. Rapid Commun.* **2002**, *23*, 896.
(29) Kawahara, M.; Rikukawa, M.; Sanui, K.; Ogata, N. *Solid State Ionics* **2000**, *136−137*, 1193.
(30) Markova, D.; Kumar, A.; Klapper, M.; Müllen, K. *Polymer* **2009**, *50*, 3411.
(31) Itoh, T.; Hirai, K.; Tamura, M.; Unoa, T.; Kubo, M.; Aihara, Y. *J. Power Sources* **2008**, *178*, 627.
(32) Park, M. J.; Nedoma, A. J.; Geissler, P. L.; Balsara, N. P.; Jackson, A.; Cookson, D. *Macromolecules* **2008**, *41*, 2271.
(33) Park, M. J.; Balsara, N. P. *Macromolecules* **2008**, *41*, 3678.
(34) Park, M. J.; Downing, K. H.; Jackson, A.; Gomez, E. D.; Minor, A. M.; Cookson, D.; Adam, Z.; Weber, A. Z.; Balsara, N. P. *Nano Lett.* **2007**, *7*, 3547.
(35) Park, M. J.; Balsara, N. P. *Macromolecules* **2009**, *42*, 6808.
(36) Park, M. J.; Balsara, N. P. *Macromolecules* **2010**, *43*, 292.
(37) Balsara, N. P.; Lin, C. C.; Dai, H. J.; Krishnamoorti, R. *Macromolecules* **1994**, *27*, 1216.
(38) Hahn, S. F. *J. Polym. Sci., Part A: Polym. Chem.* **1992**, *30*, 397.
(39) Makowski, H. S.; Lundberg, R. D.; Lundberg, G. H.; Singhal, G. H. US Patent 3870841, 1975.
(40) Knycgaka, P.; Banaszak, M.; Park, M. J.; Balsara, N. P. *Macromolecules* **2009**, *42*, 8925.
(41) Brandrup, J., Immergut, E. H., Eds.; *Polymer Handbook*, 3rd ed.; John Wiley & Sons: New York, 1989.
(42) DeLongchamp, D. M.; Vogt, B. D.; Brooks, C. M.; Kano, K.; Obrzut, J.; Richter, C. A.; Kirillov, O. A.; Lin, E. K. *Langmuir* **2005**, *21*, 11480.
(43) Fijrster, S.; Khandpur, A. K.; Zhao, J.; Bates, F. S.; Hamley, I. W.; Ryan, A. J.; Bras, W. *Macromolecules* **1994**, *27*, 6922.
(44) Matsen, M. W. *Macromolecules* **1995**, *28*, 5765.
(45) Maréchal, M.; Souqueta, J.-L.; Guindeta, J.; Sancheza, J.-Y. *Electrochem. Commun.* **2007**, *9*, 1023.

(46) Manning, G. S. *J. Chem. Phys.* **1969**, *51*, 924.
(47) Toomey, R.; Tirrell, M. *Annu. Rev. Phys. Chem.* **2008**, *59*, 493.
(48) Eisenberg, A. *Macromolecules* **1970**, *3*, 147.
(49) Yarusso, D. J.; Cooper, S. L. *Macromolecules* **1983**, *16*, 1871–1880.
(50) Earnest, T. R., Jr.; Higgins, J. S.; Handlin, D. L.; MacKnight, W. J. *Macromolecules* **1981**, *14*, 192.
(51) Fujimuia, M.; Hashimoto, T.; Kawai, H. *Macromolecules* **1981**, *14*, 1309.
(52) Peiffer, D. G.; Weiss, R. A.; Lundberg, R. D. *J. Polym. Sci., Polym. Phys. Ed.* **1982**, *20*, 1503.
(53) Eitouni, H. B.; Rappl, T. J.; Gomez, E. D.; Balsara, N. P.; Qi, S.; Chakraborty, A. K.; Fréchet, J. M. J.; Pople, J. A. *Macromolecules* **2004**, *37*, 8487.